# Theoretical Simulation and Synchrotron Excitation Spectra of Lanthanide Ions in Hexafluoroelpasolite Lattices

**ARTICLE** *in* THE JOURNAL OF PHYSICAL CHEMISTRY C · JULY 2009

Impact Factor: 4.77 · DOI: 10.1021/jp901332j · Source: OAI



**4 AUTHORS**, INCLUDING:

Chang-Kui Duan
University of Science and Technology of C…
**176** PUBLICATIONS **1,765** CITATIONS
SEE PROFILE

Peter Anthony Tanner
The Hong Kong Institute of Education
**355** PUBLICATIONS **4,286** CITATIONS
SEE PROFILE

Andries Meijerink
Utrecht University
**364** PUBLICATIONS **13,219** CITATIONS
SEE PROFILE

# Theoretical Simulation and Synchrotron Excitation Spectra of Lanthanide Ions in Hexafluoroelpasolite Lattices

**Chang-Kui Duan**[†] **and Peter A. Tanner***

*Department of Biology and Chemistry, City University of Hong Kong, Tat Chee Avenue, Kowloon, Hong Kong S.A.R., People's Republic of China*

**Vladimir Babin and Andries Meijerink**

*Debye Institute, Department of Chemistry, Utrecht University, Princetonplein 5, 3584 CC Utrecht, The Netherlands*

*Received: February 13, 2009; Revised Manuscript Received: May 5, 2009*

Vacuum ultraviolet (VUV) excitation spectra at 10 K have been recorded for the lanthanide ions, $Ln^{3+}$ = $Nd^{3+}$, $Ho^{3+}$, $Tm^{3+}$, and $Yb^{3+}$, situated at octahedral site symmetry in hexafluoroelpasolite $Cs_2NaLnF_6$ lattices. The corresponding VUV/UV/visible/near-infrared emission spectra have also been recorded. The $4f^{N-1}5d$ energy levels and $4f^N-4f^{N-1}5d$ spectral intensities have been calculated by judicious selection of parameters, without detailed fittings, when employing the M. F. Reid suite of programs. The simulations are in reasonable agreement with experimental data. Some additional spectral features for these systems have been assigned to charge transfer (CT) transitions, and CT emission is reported for the case of $Tm^{3+}$. A comparison of the results with the spectra of $LiYF_4:Ln^{3+}$ has been included and the major difference lies in the greater crystal-field strengths for $Ln^{3+}$ in the hexafluoroelpasolite lattices.



## 1. Introduction

The search for luminescent materials for mercury free fluorescent tubes, plasma display panels, vacuum ultraviolet (VUV) scintillators, or tunable ultraviolet (UV) solid-state laser materials and the availability of synchrotron radiation as excitation source has prompted extensive research of $4f^N-4f^{N-1}5d$ transitions of trivalent lanthanide ions ($Ln^{3+}$) in crystals within the past decade. Many studies have been carried out on lanthanide ions doped in fluoride crystal hosts, due to the merits of wide band gap, thermal stability, and relative inertness compared to other halide hosts. In the majority of these hosts, the lanthanide ion has been situated at a site of low symmetry. By contrast, lanthanide ions in hexafluoroelpasolite lattices ($Cs_2NaLnF_6$ or $Cs_2NaYF_6:Ln^{3+}$) occupy a high symmetry ($O_h$) site with strong crystal-field splitting of energy levels. The energy level simulation for these systems involves very few crystal-field parameters (one for 5d and two for 4f electrons only) so that the spectra are expected to be better resolved experimentally and easier to analyze theoretically. There have been some previous experimental results reported for hexafluoroelpasolite systems comprising $Pr^{3+}$,[1] $Er^{3+}$,[2] $Tm^{3+}$,[2] $Ce^{3+}$,[3,4] and $Nd^{3+}$ [5] ions and theoretical simulations were reported for $Tm^{3+}$,[6] $Pr^{3+}$,[1] and $Nd^{3+}$.[5] Here we report new vacuum ultraviolet experimental studies of hexafluoroelpasolites with $Ho^{3+}$ and $Yb^{3+}$ ions, together with some more extensitive ($Nd^{3+}$) or better resolved ($Tm^{3+}$) spectra. The theoretical simulations are also presented in detail.

## 2. Experimental Section

The hexafluoroelpasolite crystals were purchased from Prof. N. M. Khaidukov, who synthesized them by a hydrothermal method.[7] The doped concentrations of lanthanide ions are expressed in atomic % (at. %) throughout. Luminescence and excitation spectra were recorded on crystals of 1−2 mm thickness at 10 K at the HIGITI UV/VUV beamline at the DESY synchrotron in Hamburg, Germany with detection by a solar blind photomultiplier or a charge coupled device. The slit width was set so that a resolution of 2.5 nm was obtained for the excitation spectra. The experimental methods have been described previously.[8]

## 3. Theory

The rationale for assigning parameter values to simulate the energy levels and spectra is now described in detail. The parameters and their values used in the calculations are listed in Table 1.

The $4f^N$ and $4f^{N-1}5d$ multielectron energy levels were calculated by using the standard phenomenological crystal-field Hamiltonian $H(4f)$ and its extension:[9]

$$H = H(4f) + H(5d) + H_{int}(4f,5d) \quad (1)$$

where $H(4f)$, $H(5d)$, and $H_{int}(4f,5d)$ describe the interactions felt by or between the 4f electrons and felt by the 5d electron, and the interaction between 4f and 5d electrons, respectively, as shown below:

* To whom correspondence should be addressed.
[†] Present address: Institute of Modern Physics, Chongqing University of Post and Telecommunications, Chongqing 400065, People's Republic of China.

10.1021/jp901332j CCC: $40.75 
Published on Web 06/18/2009

$$H(4f) = E_{avg} + \sum_{k=2,4,6} F^k\mathbf{f}_k(f) + \zeta_{4f}\mathbf{s}_{4f}\cdot\mathbf{l}_{4f} + \sum_{i=2-4,6-8} T^k\mathbf{t}_k(f) + \alpha\mathbf{L}^2(f) + \beta\mathbf{G}(G_2(f)) + \gamma\mathbf{G}(G_7(f)) + \sum_{k=0,2,4} M^k\mathbf{m}_k(f) + \sum_{k=2,4,6} P^k\mathbf{p}_k(f) + \sum_{kq} B_q^k\mathbf{C}_q^{(k)}(f);$$

$$H(5d) = \zeta_{5d}\mathbf{s}_{5d}\cdot\mathbf{l}_{5d} + \sum_{kq} B_q^k(d)\mathbf{C}_q^{(k)}(d);$$

$$H_{int}(4f,5d) = E_{exc} + \sum_{k=2,4} F^k(fd)\mathbf{f}_k(fd) + \sum_{k=1,3,5} G^k(fd)\mathbf{g}_k(fd) \quad (2)$$

Here the italic and bold letters represent parameters and operators, respectively, and (f), (d), and (fd) are used to show that the operators are interactions for 4f electrons, the 5d electron, and interactions between 4f and 5d electrons, respectively. For $H(4f)$, $E_{avg}$ is a parameter to shift all the levels so that the energy of the lowest level of $4f^N$ is zero; the second and third terms in $H(4f)$ are the two strongest interactions for the $4f^N$ configuration ($4f^{N-1}$ core), i.e., the Coulomb and spin−orbit interactions; the last term in $H(4f)$ is the crystal-field interaction felt by 4f electrons; and the other terms are effective interactions to describe various effects due to configuration interaction. For $H(5d)$, the two terms are the spin−orbit and the strong crystal-field interactions felt by the 5d electron. For the $H_{int}(4f,5d)$ parameter, $E_{exc}$ describes the separation between the barycenters of the $4f^N$ and $4f^{N-1}5d$ levels; and the second and third terms are the direct and exchange Coulomb interaction between 4f and 5d electrons.

The crystal-field interactions felt by 4f and 5d electrons for a lanthanide ion occupying an octahedral site can be simplified to be written as:

$$H_{cf} = B_4\left[C_0^{(4)} + \sqrt{\frac{5}{14}}(C_4^{(4)} + C_{-4}^{(4)})\right] + B_6\left[C_0^{(6)} - \sqrt{\frac{7}{2}}(C_4^{(6)} + C_{-4}^{(6)})\right] \quad (3)$$

In the case of the 5d electron, only the first term needs to be included and the parameter is denoted as $B_4(d)$ in the following, to be distinguished from the one for 4f electrons, $B_4$. The total strength of the $k$th order crystal-field interactions can be defined as

$$S_k = (\sum_{q=-k}^{k} B_q^k)^{1/2} \quad (4)$$

Here for the octahedral case, $S_4 = B_4[(12/7)^{1/2}]B_4$ and $S_6 = 2(2^{1/2})B_6$.

Although both the $4f^N$ configuration and the $4f^{N-1}$ core of the $4f^{N-1}5d$ configuration contain $H(4f)$, the parameter values for these may be slightly different due to the contraction of f orbitals in the $4f^{N-1}5d$ configuration. The parameters of H(4f) for the $4f^N$ configuration were obtained from previous fittings of $4f^N$ levels, or by extrapolation from the same lanthanide ions in similar hosts. For the $4f^{N-1}5d$ core, the same parameters as for the $4f^N$ configuration were used, except for $F^k$ ($k = 2, 4, 6$) and $\zeta_{4f}$, which are enlarged from those values for the $4f^N$ configuration by the ab initio ratio 1.06 from ref 10.

**TABLE 1: The Parameters Used in the Simulation of $4f^N-4f^{N-1}5d$ Absorption Spectra**

| parameter/ion | $Nd^{3+}$ | $Ho^{3+}$ | $Tm^{3+}$ | $Yb^{3+}$ |
|---|---|---|---|---|
| $F^2$ | 72188 | 94584[a] | 101576[a] | 109800[c] |
| $F^4$ | 52625 | 67847[a] | 71602[a] | 77400[c] |
| $F^6$ | 35372 | 47274[a] | 50563[a] | 54700[c] |
| $\zeta_{4f}$ | 871 | 2130[a] | 2639[a] | 2952[a] |
| $\alpha$ | 21 | 15 | 17 | 17[c] |
| $\beta$ | −593 | −599 | −625 | −625[c] |
| $\gamma$ | 1445 | 1884 | 1820 | 1820[c] |
| $M^0$ | 2.11 | 3.00 | 1.15 | 1.15[c] |
| $P^2$ | 192 | 523 | 0 | 0[c] |
| $T^2$ | 298 | 287 | 451[b] | |
| $T^3$ | 35 | 37 | 61[b] | |
| $T^4$ | 59 | 98 | 100[b] | |
| $T^6$ | −285 | −313 | −245[b] | |
| $T^7$ | 332 | 421 | 305[b] | |
| $T^8$ | 305 | 351 | 160[b] | |
| $B_4$ | 3742 | 2756 | 2571 | 1859 |
| $B_6$ | 452 | 327 | 265 | 138 |
| $E_{exc}$ | 52000 | 83800 | 92000 | 98500 |
| $B_4(d)$ | 47300 | 44300 | 43500 | 43050 |
| $\eta_{fd}$ | 0.55 | 0.55 | 0.55 | 0.55 |
| $\zeta_{5d}$ | 1216 | 1697 | 1839 | 1910 |

[a] These values are adopted for both the $4f^N$ and $4f^{N-1}5d$ configurations, but need to be enlarged by 1.06 for the latter. [b] These values apply only to the $4f^{11}5d$ configuration, and they are from the $4f^{11}$ configuration of $Er^{3+}$. [c] These values apply only to the $4f^{12}5d$ configuration, having the factor 1.02 times the values for the $4f^{11}5d$ configuration of $Tm^{3+}$.

The cubic crystal-field parameter for the 5d electron, $B_4(d)$, was estimated by scaling the value of $B_4(d)$ for $CeCl_6^{3-}$ [11] by 1.25 (as deduced from the studies employing different halogens for $Yb^{2+}$ in MX, X = F, Cl, Br, and I[12]), and then it was decreased appropriately for each lanthanide ion by following the same trends as in $CaF_2$.[13,14] The strength of the fourth order crystal-field parameter of $Nd^{3+}$ is $S_4(d) = 61\,930\ cm^{-1}$ for the host $Cs_2NaYF_6$, which is substantially larger than $38\,567\ cm^{-1}$ for $LiYF_4$, as well as for other ions. The calculated Hartree−Fock (HF) values were used for $\zeta_{5d}$, following van Pieterson et al.[13,14]

The parameters $F^k$ (fd) ($k = 2,4$) and $G^k$ (fd) ($k = 1, 3, 5$) describe the Coulomb interaction between the $4f^{N-1}$ core and the d electron. The values used were scaled from the HF values by a factor of $\eta_{fd} = 0.55$, which was optimized from the splitting between the high-spin and the low-spin states of the $Tb^{3+}$ ion in the hexafluoroelpasolite lattice. Finally, the parameter $E_{exc}$, which describes the position of the barycenter of $4f^{N-1}$ 5d relative to that of $4f^N$, was fine-tuned to give the measured onset of $4f^N-4f^{N-1}$ 5d absorption for $Ho^{3+}$ ($N = 10$) and $Tm^{3+}$ ($N = 12$), and then it was extrapolated to $Yb^{3+}$ ($N = 13$) to predict the f−d absorption spectrum.

The $T^i$ parameters are not required for the $4f^{12}$ configuration. The $T^i$ parameters for the $4f^{11}$ core of the $4f^{11}5d$ configuration of $Tm^{3+}$ were assigned from the values for the $4f^{11}$ configuration of $Er^{3+}$, since the energy level structure of $4f^{N-1}5d$ depends only weakly on those parameters, and those parameters do not vary dramatically across the lanthanide ion series. There are no $F^k$ ($k = 2, 4, 6$) parameters for the $4f^{13}$ configuration of $Yb^{3+}$. Hence for the $4f^{12}$ core of the $4f^{12}5d$ configuration, the values were derived by scaling the values for the $4f^{11}$ core of the $4f^{11}5d$ configuration of $Tm^{3+}$ with the ab initio value 1.02 derived from ref 10.

The transitions between $4f^N$ and $4f^{N-1}5d$ are electric dipole allowed and it is straightforward to calculate the matrix elements of the electric dipole moment operator between multielectron

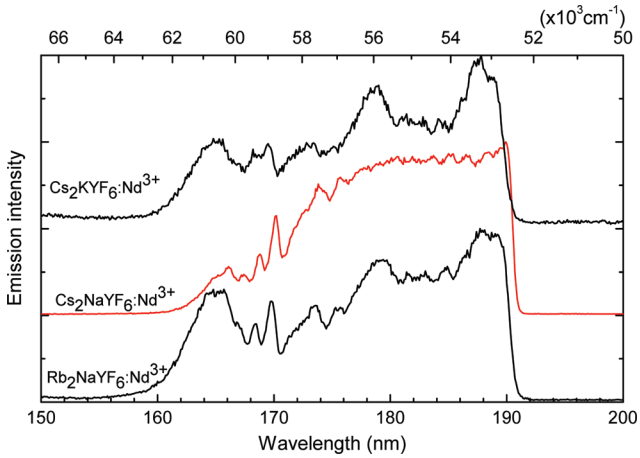


**Figure 1.** Excitation spectra of $Nd^{3+}$ in hexafluoroelpasolites at 10 K, monitoring the emission from the $4f^3\ ^2G(2)_{9/2}$ level at 287−289 nm. Spectra are shifted vertically for clarity. The concentrations of $Nd^{3+}$ are 1 at. % in each case.

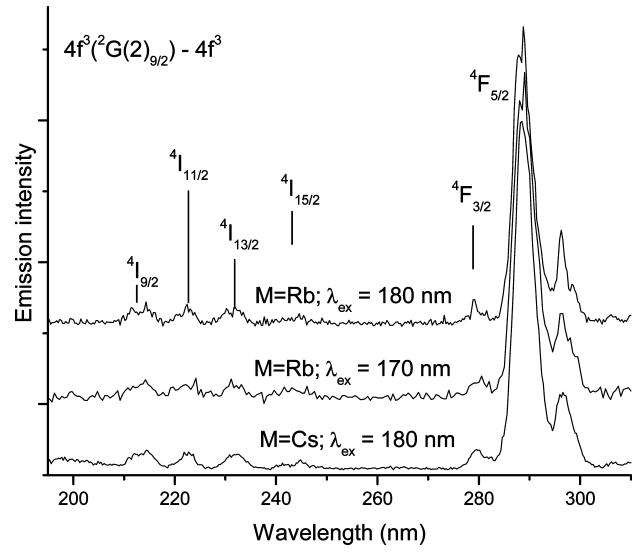


**Figure 2.** Emission spectra between 195 and 310 nm at 10 K of $M_2NaYF_6:Nd^{3+}$ (M = Rb, Cs; the concentration of Nd is 1 at. %) under different excitation lines. Spectra are shifted vertically for clarity. The terminal $4f^3$ multiplet terms are marked.

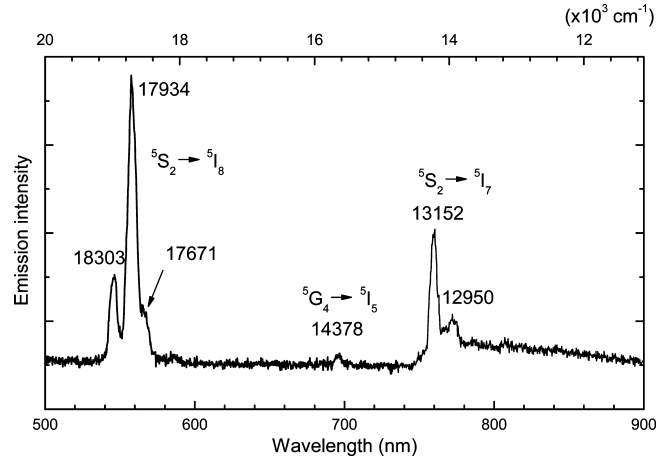


**Figure 3.** Emission spectrum at 10 K of $Cs_2NaYF_6:Ho^{3+}$ (10 at. %) excited at 160 nm.



wave functions of $4f^N$ and $4f^{N-1}5d$. Since the interaction of 5d orbitals is different from (and much stronger than) that of 4f orbitals, there is generally a displacement for the equilibrium positions of ligands. Such a displacement results in the broad bands and consequently large Stokes shifts of vibronic structure of the absorption and emission spectra. Since the detailed vibronic structures are not always well-resolved, the crude simulation of them proposed by Reid et al.[9] was adopted, i.e., by using Gaussian curves, displaced toward higher energy from the zero-phonon lines by $E_{shift} = 600\ cm^{-1}$ and $E_{width} = 1000\ cm^{-1}$, as estimated from the experimental spectra. The package written by Prof. M. F. Reid was used to perform all the calculations.

## 4. Results and Discussion

The following results present the VUV excitation and emission spectra of the ions $Nd^{3+}$, $Ho^{3+}$, $Tm^{3+}$, and $Yb^{3+}$ in hexafluoroelpasolite lattices, as now described one by one.

**4.1. $Nd^{3+}$.** Figure 1 shows the excitation spectra for $Cs_2KYF_6:Nd^{3+}$, $Cs_2NaYF_6:Nd^{3+}$, and $Rb_2NaYF_6:Nd^{3+}$ (where the dopant ion concentration in each case is 1 at. %), by monitoring the $4f^3-4f^3$ emission located near 290 nm. All three spectra exhibit broad $4f^3-4f^25d$ absorption between 160 and 192 nm, with the structure mainly due to splitting of the $4f^2$ core by Coulomb interaction (i.e., the separation between $^3F$ and $^3H$) and spin−orbit interaction. The spectrum of $Cs_2NaYF_6:Nd^{3+}$ is not as well-resolved as the others, and there is a slight higher energy shift for $Cs_2KYF_6:Nd^{3+}$ (by 250 $cm^{-1}$) and $Rb_2NaYF_6:Nd^{3+}$ (by 80 $cm^{-1}$) relative to the spectrum of $Cs_2NaYF_6:Nd^{3+}$. The previous calculation[5] explained the low energy part of the measured f−d absorption spectrum very well. However, the parameter value $B_4(d) = 38\ 220\ cm^{-1}$ used in ref 5 is even smaller than the value $B_4(d) = 38\ 709\ cm^{-1}$ for $Cs_2NaYCl_6:Ce^{3+}$ [11] and is therefore too small. Actually, the simulation of the 160−192 nm region of the absorption spectrum is rather insensitive to the value of $B_4(d)$ so that the calculated f−d absorption spectrum in this range using the parameters given here is almost the same as that in ref 5. Higher energies are predicted herein for levels where the 5d electron is in the higher crystal-field component $e_g$. Upon the basis of the calculated energies, the weak absorption in the range 130−145 nm reported in ref 5 (also observed herein, but not shown in Figure 1) is assigned to low-spin (spin $^1/_2$) states $^2[^3H\ ^2(t_{2\ g})]$ (where the symbols denote the $4f^2$ core and 5d-electron states). The 5d $e_g$ absorptions are estimated to spread from 132 nm to shorter wavelengths but are expected to be very weak due to ionization, The charge-transfer (CT) absorption $Nd^{3+}-Cl^-$ is estimated to be at 120 nm using the method given by Dorenbos and the CT absorption wavelength 154 nm for $Eu^{3+}$ in the $LiCaAlF_6$ host.[15] The broad peak at 120 nm (also observed, but not shown in Figure 1) is more likely assigned to the host exciton transition.

Figure 2 shows the emission spectra of $Nd^{3+}$ in hexafluoroelpasolites under VUV excitation and is similar to the previously reported spectra.[5] The interconfigurational transitions are not observed herein, but have previously been reported when using a 40 ns time window.[5] The relative intensities of the $4f^3-4f^3$ transitions are much stronger for transitions to terminal $^4F$ than $^4I$ multiplet terms, with the strongest band being the $^2G(2)_{9/2} \rightarrow {}^4F_{5/2}$ transition with its maximum at 288 nm.

**4.2. $Ho^{3+}$.** Figure 3 shows the emission spectrum of $Cs_2NaYF_6:Ho^{3+}$ (10 at. %) under the excitation of 160 nm synchrotron radiation. The major bands are assigned to the emission from the $^5S_2$ multiplet term to $^5I_8$ and $^5I_7$ levels. The assignment is based on the fact that in $Cs_2NaYCl_6$ the lowest level of the $^5S_2$ multiplet is at 18 365 $cm^{-1}$ and it is expected to be at a fairly similar energy in $Cs_2NaYF_6$. The gap of ca. 2800 $cm^{-1}$ below

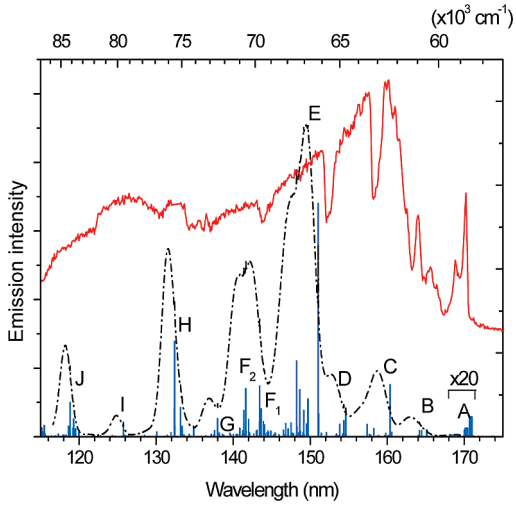


**Figure 4.** Excitation spectrum of $Cs_2NaYF_6$:$Ho^{3+}$ (10 at. %) by monitoring the emission at 557 nm. Refer to the text for the explanation.

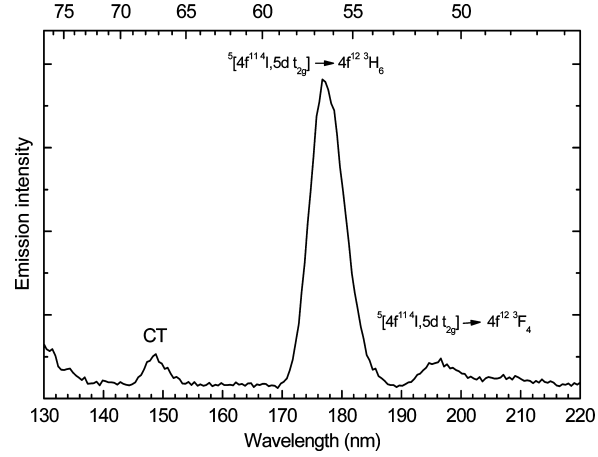


**Figure 5.** Emission spectrum of $Cs_2NaYF_6$:$Tm^{3+}$ (1 at. %) at 10 K, using 127.5 nm radiation.

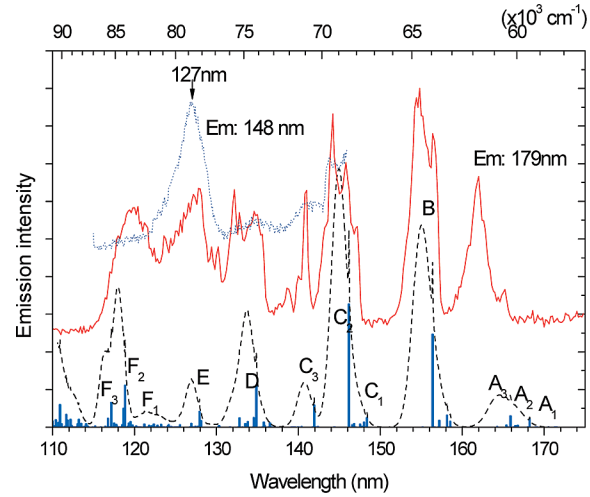


**Figure 6.** Excitation spectra of $Cs_2NaYF_6$:$Tm^{3+}$ (10 at. %) at 10 K by monitoring 179 and 148 nm emission bands, and (lower sticks and convolution) simulation of $4f^{12} \rightarrow 4f^{11}5d$ absorption spectrum. Refer to the text for the explanation.



$^5S_2$ makes the emission from this level possible. The separation of ca. 5150 $cm^{-1}$ between the two groups agrees with the separation between $^5I_8$ and $^5I_7$, which is 5117 $cm^{-1}$ in $Cs_2NaYCl_6$. The weak band at 14 378 $cm^{-1}$ between the two groups does not correspond to emission from $^5F_5$, but is alternatively assigned to the $^5G_4 \rightarrow {}^5I_5$ transition, inferring that $^5G_4$ is located at ~25 900 $cm^{-1}$.

Figure 4 (upward-shifted solid curve) shows the excitation spectra for this system by monitoring the $^5S_2 \rightarrow {}^5I_8$ emission. The calculated $4f^{11}-4f^95d$ absorption line strength is shown below, with the zero-phonon lines represented by sticks and the convolution by the dashed-dot curve. Due to the saturation, the incident radiation is almost totally absorbed near the surface and the excitation spectrum does not show much structure except for the excitation into the high-spin $4f^95d$ states (around 170 nm) where the absorption is weak due to the spin-forbidden nature of the transitions.

Since most of the vibronic bands are not well-resolved, the convolution was performed by following the method given by Prof. M. F. Reid, as described above. The calculation is enlarged by a factor of 20 for better display in the range 167−175 nm. The calculated $4f^95d$ levels start at 57 600 $cm^{-1}$, and the zero-phonon line for the first resolvable absorption peak is at ca. 171 nm (58 500 $cm^{-1}$). The capital letters A−J denote the locations of terminal $4f^95d$ multiplet terms. The regions A−D are dominated by high-spin $^7[(^6H)t_{2g}]$; E−G by low-spin $^5[(^6H)t_{2g}]$; and H by $^5[(^6F)t_{2g}]$. The region I, corresponding to $^7[(^6H)e_g]$, may not be efficient for excitation since delocalization of $e_g$ orbitals occurs due to the presence of resonant conduction band states. The region J is a mixture of $^5[(^4F(3))t_{2g}]$ and $^7[(^6H)e_g]$. Generally, the simulation is not in good agreement with the excitation spectrum except for the low-energy region, but saturation effects distort the region between 120 and 160 nm.

The excitation spectrum also comprises, at lower energy, a broad band centered at 210 nm (not shown in Figure 4). This feature is associated with oxyfluoride impurities. Excitation into this broad band by using 215 nm radiation gave a broad, structured emission band between 500 and 800 nm.

**4.3. $Tm^{3+}$.** Figure 5 shows the emission spectrum of $Tm^{3+}$ in $Cs_2NaYF_6$ (1 at. %) using 127.5 nm synchrotron radiation excitation. The emission under 120 nm excitation is similar and is not shown here. Apart from the well-known strong emission from the high-spin $4f^{11}5d$ states with maximum intensity at ca. 179 nm,[6] there is a weaker broad band at 148 nm. The excitation spectra monitoring both of the 179 and 148 nm emission bands are shown in Figure 6 together with calculated 4f−5d absorption line strengths.

The parameters used in the calculation are slightly different from those in ref 6 but the pattern of the calculated absorption spectrum is almost the same. The calculated $4f^{11}5d$ levels start at 58 300 $cm^{-1}$ (171.5 nm) and spread up to much more than $10^5$ $cm^{-1}$. The terminal states in Figure 6 are again designated by letters. The bands $A_1-A_3$, $C_1$, and $C_3$ are dominated by high-spin states $^5[(^4I)t_{2g}]$; B, $C_2$, and D are dominated by low-spin final states $^3[(^4I)t_{2g}]$; E is $^3[(^4F)t_{2g}]$; $F_1$ and $F_3$ are $^3[(^2H(2))t_{2g}]$; and $F_2$ is $^3[(^4I)e_g]$. The gaps in the absorption spectrum are actually filled with other $4f^{11}5d$ states with weak absorption. The weak emission band at 148 nm may be due to emission either from the $C_1$ high-spin $4f^95d$ state or from the CT state. Alternative assignments were discussed by Makhov et al.[2] In view of the many closely spaced fd states between the $C_1$ and B states, the 148 nm emission band is unlikely to be due to $4f^95d-4f^{10}$ emission and it is attributed to emission from $Tm^{3+}$ CT states, i.e., the transition initial state is the ground state of $Tm^{2+}$ together with a hole in the valence band, and the final states are low-lying states of $Tm^{3+}$ together with a filled valence band. The charge transfer states have a different potential

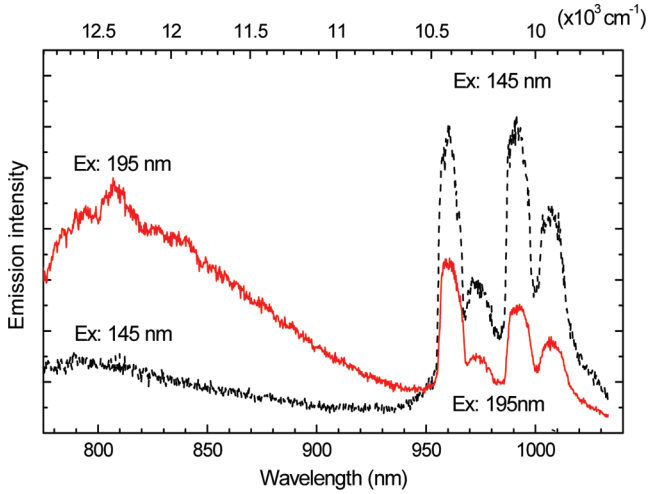


**Figure 7.** Emission spectra at 10 K of $Cs_2NaYF_6:Yb^{3+}$ (10 at. %) with synchrotron radiation excitation at 145 and 195 nm. The emission intensities are arbitrary.

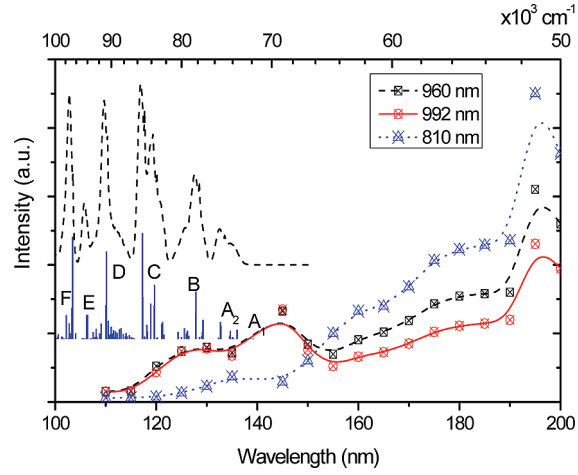


**Figure 8.** Excitation spectra of $Cs_2NaYF_6:Yb^{3+}$ (10 at. %) at 10 K and simulated $4f^{13} \rightarrow 4f^{12}5d$ absorption spectrum. Refer to the text for the explanation.



minimum distribution in the configuration coordinate diagram and presumably the potential barrier between CT states and $4f^{N-1}5d$ states prevents to some extent the nonradiative relaxation of CT states to $4f^{N-1}5d$ states and thus enables emission to occur. It can also be seen from Figure 6 that the excitation spectra for the emission bands at 148 and 179 nm are different. This is because the excitation for 148 nm emission is due to CT absorption, whose peak is 127 nm (which is the same wavelength as predicted by using the method given by Dorenbos[15]). Part of the excitation for 179 nm emission near 127 nm in Figure 6 may also be due to CT absorption. The $Tm^{3+}-F^-$ CT absorption band has been distinguished from excitonic absorption and assigned at similar energy to that herein in the spectra of $Tm^{3+}$-doped $LiSrAlF_6$[16] and $LiCaAlF_6$.[17]

**4.4. $Yb^{3+}$.** Figure 7 shows the emission of $Cs_2NaYF_6:Yb^{3+}$ (10 at. %) under 145 and 195 nm excitation. The emission peaks in the range 950−1020 nm are due to emission from the lowest energy crystal-field level of $4f^{13}\ ^2F_{5/2}$ to the crystal-field levels of the $4f^{13}\ ^2F_{7/2}$ multiplet, as shown under higher resolution in the 2 K spectrum of ref 18. The two strongest peaks are magnetic dipole transitions to the lowest two crystal-field levels $\Gamma_8$ and $\Gamma_7$, respectively. Apart from the $4f^{13}-4f^{13}$ emissions, there is a broad band around ca. 810 nm that cannot be ascribed to any known transitions of $Yb^{3+}$ in this host.[18,19]

The excitation spectra were measured by monitoring the intensities of the two peaks at 960 and 992 nm under selected excitation lines, as well as that of the anomalous emission at 810 nm. These spectra are presented in Figure 8 together with the calculated $4f^{13}-4f^{12}5d$ absorption spectrum. In the $Cs_2NaYF_6$ host, the $4f^{13}-4f^{12}5d$ absorption of $Yb^{3+}$ is predicted to start at the energy around 71 000 $cm^{-1}$ (~141 nm). Peak $A_1$ is $^4[4f^{12}\ ^3H, t_{2g}]$; peaks $A_2$, B, C, E, and F are spin-mixed states of $[^4f^{12}\ ^3H, t_{2g}]$; and peak D corresponds to transitions to spin-mixed states of $[^4f^{12}\ ^3F, t_{2g}]$.

The $F^-Yb^{3+}$ CT band is estimated to start at ca. 68 600 $cm^{-1}$ (146 nm), with an uncertainty of a few $10^3$ $cm^{-1}$. The CT wavelength of $Yb^{3+}$ in $LiYF_4$ is listed as 159 nm.[20,21] Hence the 145 nm band in the excitation spectra, Figure 8, can be ascribed to CT absorption.

Although hexafluoroelpasolites are more stable in air than the corresponding hexachloroelpasolites, the prolonged exposure of the $Cs_2NaYF_6:Yb^{3+}$ sample to air may result in $O^{2-}$ impurities in the sample. The $O^{2-}-Yb^{3+}$ CT absorption was observed to be lower than the $F^-Yb^{3+}$ CT absorption by ca. 21 000 $cm^{-1}$ in $YF_3$ or $LaF_3$ doped with $Eu^{3+}$, $Dy^{3+}$, or $Er^{3+}$ ions.[22] This gives a prediction of ca. 48 000 $cm^{-1}$ for the present case of the $O^{2-}-Yb^{3+}$ CT absorption. Within the uncertainties of a few $10^3$ $cm^{-1}$, the strong excitation band at 51 300 $cm^{-1}$ (195 nm) is close to the prediction, and is very likely to be CT absorption from $O^{2-}$ impurities to $Yb^{3+}$ ions. It is interesting that the excitation spectrum for the anomalous 810 nm emission does not contain the $F^-Yb^{3+}$ CT band, but does contain the $O^{2-}-Yb^{3+}$ CT absorption band. This indicates that the 810 nm emission is related to $O^{2-}$ impurities.

## 5. Conclusions

The VUV excitation and VUV/UV/visible/near-IR emission spectra of $Ln^{3+} = Nd^{3+}$, $Ho^{3+}$, $Tm^{3+}$, and $Yb^{3+}$ in hexafluoroelpasolite lattices have been recorded at 10 K. The bandgap of the $Cs_2NaYF_6$ host is sufficiently high in energy so that $4f^N-4f^{N-1}5d$ excitation spectra of $Ln^{3+}$ can be observed. These transitions are electric dipole allowed. Generally, the spectra comprise structured, broad bands at the resolution of several nanometers employed, due to the congestion of energy levels and the occurrence of unresolved vibronic structure. For comparison with the experimental excitation spectra, the simulations of $4f^N-4f^{N-1}5d$ absorption spectra have been carried out with most of the parameters being assigned numerical values by comparison with other systems, rather than by an optimized fitting of the experimental data. The simulated spectra are in reasonable agreement with experiment except for some additional bands which are assigned to CT transitions. The $F^-Ln^{3+}$ CT energies of the systems studied follow similar trends to the analogous CT energies of the $LnCl_6^{3-}$ series,[23] with $Tm^{3+}$ (78 802 $cm^{-1}$) > $Yb^{3+}$ (68 587 $cm^{-1}$). Using $4f^N-4f^{N-1}5d$ excitation, $4f^N-4f^N$ emission was reported for $Nd^{3+}$, $Ho^{3+}$, and $Yb^{3+}$ and $4f^{N-1}5d-4f^N$ and CT emissions were reported for $Tm^{3+}$.

It is instructive to compare the present results with those for the $LiYF_4:Ln^{3+}$ systems.[14,24] The Slater parameters herein are smaller but within 10% of the latter values. The crystal-field parameters for the f and d electrons are totally different, not only in magnitude but also in sign, from the corresponding values used to model the energy levels in $D_{2d}$ symmetry. The $4f^{N-1}5d \rightarrow 4f^N$ emission spectra of $Nd^{3+}$[5] and $Tm^{3+}$ in hexafluoroelpasolite lattices are similar to the spectra of these ions in $LiYF_4$ in that the major intensity is in the transitions to

terminal $^4I_J$ and $^3H_6$ multiplets, respectively. A high-energy emission band around 148 nm is assigned to CT emission from $Tm^{3+}$.

There are striking differences in the excitation spectra for $Ln^{3+}$ in $Cs_2NaYF_6$ and in $LiYF_4$. For $Nd^{3+}$, the group of bands between 160 and 190 nm is more structured in the former case, but the higher energy bands between 160 and 120 nm are much weaker.[5] Our absorption line strength calculations, or those of ref 5, predict higher intensities for these bands in $Cs_2NaYF_6$:$Nd^{3+}$. Nonradiative relaxation from the higher energy states is evidently ineffective for population of the luminescent state. Although saturation effects due to the high dopant ion concentration of $Tm^{3+}$ employed herein cannot be excluded, the relative intensity of transitions to high spin states is apparently much greater in the case of $Cs_2NaYF_6$:$Tm^{3+}$ than $LiYF_4$:$Tm^{3+}$. This could arise from the smaller splitting between high−low spin states due to smaller exchange interaction parameters between 4f and 5d orbitals for the former system. The major peaks A, B (with a separation of 6090 $cm^{-1}$) in Figure 15 of ref 14 are more widely separated than the peaks B, C herein (Figure 6, ~5000 $cm^{-1}$); the sharp peak D in Figure 15 of ref 14 has a counterpart in $C_3$. Those separations originate from the core splitting $^4I_J$ due to 4f spin−orbit interaction.

**Acknowledgment.** Financial support for this work under the Hong Kong Research Grants Council GRF research grant CityU 102308 is gratefully acknowledged. C.K.D. is partially supported by the National Science Foundation of China, under Grant No. 10874253.

## References and Notes

(1) Schiffbauer, D.; Wickleder, C.; Meyer, G.; Kirm, M.; Stephan, M.; Schmidt, P. C. *Z. Anorg. Allg. Chem.* **2005**, *631*, 3046.
(2) Makhov, V. N.; Khaidukov, N. M.; Lo, D.; Krupa, J. C.; Kirm, M.; Negodin, E. *Opt. Mater.* **2005**, *27*, 1131.
(3) Aull, B. F.; Jenssen, H. P. *Phys. Rev. B* **1986**, *34*, 6640.
(4) Aull, B. F.; Jenssen, H. P. *Phys. Rev. B* **1986**, *34*, 6647.
(5) Tanner, P. A.; Ning, L.; Makhov, V. N.; Khaidukov, N. M.; Kirm, M. *J. Phys. Chem. B* **2006**, *110*, 12113.
(6) Ma, C.; Tanner, P. A.; Xia, S.; Yin, M. *Opt. Mater.* **2007**, *29*, 1620.
(7) Tanner, P. A.; Liu, Y.-L.; Edelstein, N.; Murdoch, K.; Khaidukov, N. M. *J. Phys.: Condens. Matter* **1997**, *9*, 7817.
(8) Wegh, R. T.; Meijerink, A. *Phys. Rev. B* **1999**, *60*, 10820.
(9) Reid, M. F.; van Pieterson, L.; Wegh, R. T.; Meijerink, A. *Phys. Rev. B* **2000**, *62*, 14744.
(10) Reid, M. F.; van Pieterson, L.; Meijerink, A. *J. Alloys Compd.* **2001**, *344*, 240.
(11) Tanner, P. A.; Mak, C. S. K.; Edelstein, N. M.; Liu, G.; Huang, J.; Seijo, L.; Barandiaran, Z. *J. Am. Chem. Soc.* **2003**, *125*, 13225.
(12) Duan, C. K.; Tanner, P. A. *J. Phys.: Condens. Matter* **2008**, *20*, 215228.
(13) van Pieterson, L.; Reid, M. F.; Wegh, R. T.; Soverna, S.; Meijerink, A. *Phys. Rev. B* **2002**, *65*, 045113.
(14) van Pieterson, L.; Reid, M. F.; Burdick, G. W.; Meijerink, A. *Phys. Rev. B* **2002**, *65*, 045114.
(15) Dorenbos, P. *J. Phys.: Condens. Matter* **2003**, *15*, 8417.
(16) True, M.; Kirm, M.; Negodine, E.; Vielhauer, S.; Zimmerer, G. *J. Alloys Compd.* **2004**, *374*, 36.
(17) True, M.; Chen, Y.; Kirm, M.; Vielhauer, S.; Zimmerer, G. *J. Lumin.* **2007**, *124*, 279.
(18) Falin, M. L.; Gerasimov, K. I.; Leushin, A. M.; Khaidukov, N. M. *J. Lumin.* **2008**, *128*, 1103.
(19) Zhou, X.; Reid, M. F.; Faucher, M. D.; Tanner, P. A. *J. Phys. Chem. B* **2006**, *110*, 14939.
(20) Li, L.; Zhou, S.; Zhang, S. *J. Lumin.* **2009**, *129*, 187.
(21) van Pieterson, L.; Heeroma, M.; de Heer, E.; Meijerink, A. *J. Lumin.* **2000**, *91*, 177.
(22) Gerard, I.; Krupa, J. C.; Simoni, E.; Martin, P. *J. Alloys Compd.* **1994**, *207*, 120–127.
(23) Ionova, G.; Krupa, J. C.; Gerard, I.; Guillaumont, R. *New J. Chem.* **1995**, *19*, 677.
(24) van Pieterson, L.; Wegh, R. T.; Meijerink, A.; Reid, M. F. *J. Chem. Phys.* **2001**, *115*, 9382.

JP901332J